Role of the Extracellular Loop in the Folding of a CFTR Transmembrane Helical Hairpin†

Hania Wehbi, Arianna Rath, Mira Glibowicka, and Charles M. Deber*

Division of Molecular Structure and Function, Research Institute, Hospital for Sick Children, 555 University Avenue, Toronto, Ontario M5G 1X8, Canada, and Department of Biochemistry, University of Toronto, 1 King's College Circle, Toronto, Ontario M5S 1A8, Canada

Received December 14, 2006; Revised Manuscript Received April 9, 2007

ABSTRACT: The folding of membrane-spanning domains into their native functional forms depends on interactions between transmembrane (TM) helices joined by covalent loops. However, the importance of these covalent linker regions in mediating the strength of helix−helix associations has not been systematically addressed. Here we examine the potential structural impact of cystic fibrosis-phenotypic mutations in the extracellular loop 2 (ECL2) on interactions between the TM3 and TM4 helices of the cystic fibrosis transmembrane conductance regulator (CFTR) in constructs containing CFTR residues 194−241. When the effects of replacements in ECL2 (including the CF-phenotypic mutants E217G and Q220R) were evaluated in a library of wild-type and mutant TM3-ECL2-TM4 hairpin constructs, we found that SDS−PAGE gel migration rates differed over a range of nearly 40% +/− the wild-type position and that decreased migration rates correlate with increasing hairpin α-helical content as measured by circular dichroism spectra in sodium dodecyl sulfate micelles. The decreased mobility of TM3/4 constructs by introduction of non-native residues is interpreted in terms of an elongation or "opening" of the helical hairpin and concomitant destabilization of membrane-based helix−helix interactions. Our results support a role for short loop regions in dictating the stability of membrane protein folds and highlight the interplay between membrane-embedded helix−helix interactions and loop conformation in influencing the structure of membrane proteins.

Membrane proteins comprise 20−30% of the total number of proteins contained in genomes of various organisms (*1*, *2*). This class of proteins represents prime targets in pharmaceutical research, as membrane proteins are estimated to comprise approximately 70% of current drug targets (*3*). Mutations in membrane proteins are also the lead causes of various genetic diseases such as cystic fibrosis (*4*). The experimental challenges associated with the hydrophobic nature of membrane proteins, however, have impeded our understanding of their structure/function relationships. Membrane proteins represent only ∼0.3% of the >34000 structures deposited in the Protein Data Bank (*5*), and fewer than 100 membrane protein structures have been solved to high resolution (*6*). Though it has been noted that the structural characterization of membrane proteins is moving forward exponentially (*7*), at the present pace of structural determinations it still may take more than 3 decades to obtain representative structures of most membrane protein folds (*5*).

The folding of α-helical membrane proteins has been modeled as a two-stage process (*8*, *9*), where the first step involves the insertion of hydrophobic TM[1] segments into the interior of lipid bilayer, and the second step involves the formation of tertiary contacts between TM α-helices. The two-stage model implies that each TM segment behaves as an individual folding unit and that helix−helix interactions have sufficient specificity to generate membrane protein folds. While this model does not specifically address the role(s) of the extramembranous loop regions that connect TM helices in guiding membrane protein folding, its underlying principles have been supported by studies of bacteriorhodopsin (bR) and other membrane proteins. The native bR fold, for instance, can be regenerated from various protein fragments with severed or deleted connecting loops (*10*−*13*). Loop-severed or -deleted fragments of other α-helical membrane proteins such as rhodopsin (*14*), muscarinic acetylcholine receptor (*15*), yeast α-factor transporter (*16*), and lactose permease (*17*) are also capable of reassembling via helix−helix interactions into native or near-native conformations.

† This work was supported, in part, by grants to C.M.D. from the Canadian Cystic Fibrosis Foundation (CCFF) and the Canadian Institutes of Health Research (CIHR). H.W. held a postdoctoral fellowship award from the CIHR Strategic Training Program in Structural Biology of Membrane Proteins Linked to Disease. A.R. holds a postdoctoral fellowship award from the CIHR Strategic Training Program in Protein Folding: Principles and Diseases.

* Address correspondence to this author at the Hospital for Sick Children. Phone: 416-813-5924. Fax: 416-813-5005. E-mail: deber@sickkids.ca.

[1] Abbreviations: bR, bacteriorhodopsin; CD, circular dichroism; CF, cystic fibrosis; CFTR, cystic fibrosis transmembrane conductance regulator; ECL, extracellular loop; ICL, intracellular loop; PAGE, polyacrylamide gel electrophoresis; SDS, sodium dodecyl sulfate; TM, transmembrane; TM3/4, helical hairpin including residues 194−241 of CFTR; TMD, transmembrane domain; WT, wild type.

10.1021/bi602570u CCC: $37.00
Published on Web 05/22/2007

However, membrane proteins reconstituted from helix−helix interactions alone do not always recover wild-type (WT) stability and/or function. For example, bR proteins assembled from fragments, or designed with non-natural covalent loop sequences, typically exhibit lower than WT stability and/or altered functional properties (*18*−*22*). Certain loop regions are additionally capable of forming defined tertiary structures when excised from the full-length protein (*23*−*27*), implying that these regions can contribute favorably to the overall stabilization of membrane protein structures.

Several mutations that cause cystic fibrosis (CF) have been localized to various connecting loops of the cystic fibrosis transmembrane conductance regulator (CFTR), a chloride channel located in the apical membrane of epithelial cells. The CFTR molecule contains 12 TM helices linked by four intracellular loops (ICLs) and six extracellular loops (ECLs) (reviewed in ref *28*). The ICLs significantly exceed the ECLs in length and are implicated in long-range interactions between the membrane and cytoplasmic domains. CF-associated mutations in ICL1, ICL2, ICL3, and ICL4 cause the protein to be misprocessed and/or display altered chloride channel activity (*29*−*31*), and the secondary structure of ICL4 in particular has been postulated to contribute crucially to the proper folding of the entire CFTR molecule (*31*). Although CF-causing mutations in the ECLs generally allow for proper processing of CFTR, most seriously compromise its chloride channel activity, indicating that the ECLs contribute to the stability of the CFTR ion pore (*32*). These results are remarkable given that ECLs are generally quite short (approximately 5−30 residues) and might therefore be expected to participate predominantly in local, rather than long-range, stabilizing interactions.

Using a helix−loop−helix segment of CFTR corresponding to TM helix 3, ECL2, and TM helix 4 (termed TM3/4), we have previously shown in vitro that a CF-phenotypic point mutation in the CFTR TM helix 4 induces non-native helix−helix interactions that could alter the normal assembly and alignment of CFTR TM helices and/or impede their movement in response to substrate transport (*33*). However, the potential role(s) of ECLs in stabilizing the biologically relevant conformation of CFTR has (have) not been systematically characterized. Here we extend our examination of the molecular basis of CF by examining the effect of point mutations in ECL2 on the folding of the TM3/4 hairpin.

EXPERIMENTAL PROCEDURES

TM Prediction. The boundaries of the TM3 helix and TM4 helix of CFTR were identified by submission of residues 190−247 of the *Homo sapiens* CFTR sequence to the web-based program TM Finder (www.bioinformatics-canada.org/TM/) (*34*) using all default parameters except gap length, which was set to 5.

Expression and Purification of TM3/4 Constructs of CFTR. The cDNAs encoding *H. sapiens* CFTR residues 194−241 were subcloned into the pET32a vector following procedures adapted from Peng et al. (*35*). The resulting construct, designated TM3/4 WT in this work, contains a C225A replacement designed to prevent disulfide bond formation between different helical hairpin molecules, has a 32-residue N-terminal fusion with an S-tag epitope used for Western blot detection (sequence GSGMKETAAAKFERQHMDSPDLGTDDDDKAM), and has an 8-residue C-terminal fusion with the hexahistidine tag used for purification by affinity chromatography (sequence LEHHHHHH). TM3/4 mutants were generated using the QuikChange site-directed mutagenesis kit (Stratagene). Expression and purification of all TM3/4 constructs was performed as previously described (*33*, *35*−*38*).

Sodium Dodecyl Sulfate−Polyacrylamide Gel Electrophoresis (SDS−PAGE) Analysis of TM3/4 Constructs. Purified TM3/4 constructs were run on SDS−PAGE and their migration rates compared to that of the TM3/4 WT protein as described (*33*, *38*). Briefly, the percent change in molecular weight (MW) was first calculated from gels by comparing the apparent MW of each TM3/4 hairpin [estimated from the migration rates of Mark-12 molecular weight markers (Invitrogen)] to its expected theoretical MW using the equation:

$$\%\ \text{change} = \frac{(\text{theoretical MW} - \text{apparent MW}) \times 100}{\text{theoretical MW}}$$

The percent change in MW of each ECL2 replacement in the TM3/4 WT or TM3/4 V232D backgrounds was then normalized to the migration of the parental hairpin as follows:

$$\%\ \text{change vs TM3/4 parent} = \frac{(\%\ \text{change TM3/4 parent} - \%\ \text{change ECL2 mutant}) \times 100}{\%\ \text{change TM3/4 parent}}$$

ECL2 mutants with positive percent changes thus migrate less than their parental hairpin on SDS−PAGE; those with negative values migrate further.

Circular Dichroism (CD) Spectroscopy. Lyophilized samples of purified WT or mutant TM3/4 hairpins were resuspended in 25 mM SDS and 10 mM Tris, pH 7.5, to yield a final TM3/4 concentration of 20 μM. CD spectra were collected on a Jasco J-720 circular dichroism spectropolarimeter. Following spectra collection, CD samples were diluted 20-fold using water to render the SDS concentration compatible with the BCA protein determination method. Protein concentrations in each CD sample were then verified using the Micro BCA assay (Pierce).

RESULTS

Definition of ECL2 Boundaries. Loop boundaries are typically defined by determining the limits of the successive TM segments that they connect. At the time of the discovery of the relationship of CFTR to CF disease, the ECL2 that connects the TM3 and TM4 helices in CFTR was schematically depicted as consisting of five residues with the sequence ^{216}WELLQ^{220} (*39*). More recently using TM Finder, a TM prediction program developed in our laboratory that predicts TM regions based on experimentally determined helicity and hydrophobicity values in apolar solvents (*34*), we find one apparently uninterrupted TM segment without a clearly defined connecting loop in this region of the *H. sapiens* CFTR sequence (Figure 1). However, the near-baseline decrease in both helicity and hydrophobicity of the region between residues 220−226 (Figure 1) earmarks this region as the potential connecting loop (*34*). Other TM helix prediction programs have designated residues 217−219 as the ECL2 region (*40*). We decided to encompass the previous designations as well as our prediction for the purposes of

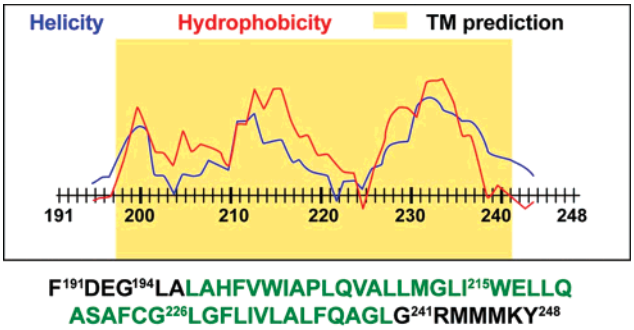

FIGURE 1: Prediction of transmembrane segments in CFTR residues 190−247. The yellow background reflects potential transmembrane region(s). The CFTR sequence used in the prediction is given below the graph. Residues displayed in green reflect the transmembrane region of TM3/4 predicted by TM Finder (*34*). The TM3/4 construct contains residues 194−241. Residues considered as the ECL2 in this study span Ile 215 to Gly 226.

the present work and utilized an inclusive definition of ECL2 as TM3/4 WT residues ^{215}IWELLQASAFAG^{226}.

Analysis of CF-Phenotypic ECL2 Mutations in the TM3/4 WT Background. Two CF-phenotypic missense mutations, E217G and Q220R, have been documented in the ECL2 region (contributed to the Cystic Fibrosis Mutation Database at www.genet.sickkids.on.ca/cftr/ by Zielenski et al. and Férec). These charged-to-uncharged and polar-to-charged mutations can perturb such parameters as the net charge, side chain volume, hydrophobicity, and residue helical propensity of ECL2 and might therefore also perturb the normal structure of the TM3/4 WT hairpin, possibly by the disruption of wild-type extant van der Waals and/or side chain−side chain electrostatic interactions (*33*, *41*). E217G and Q220R point mutants were constructed initially in the TM3/4 WT background, and their migration on SDS−PAGE was compared to WT following the gel shift assay developed in our laboratory (*33*). This assay assesses the mutation-dependent migration of TM3/4 constructs, where more tightly folded hairpins migrate faster than WT and vice versa (*33*, *38*). We noted that the E217G and Q220R substitutions in the WT background each showed *slower* migration relative to WT on SDS−PAGE (Figure 2), initially implying that replacement of these ECL2 positions has rendered the TM3/4 WT construct less compact (vide infra).

Substitutions at E217 Have Variable Effects on TM3/4 WT Folding. The formation of non-native side chain−side chain electrostatic interactions by membrane-based polar mutants has been postulated to alter TM3/4 folding and dynamics (*33*). In the present work, we sought to examine the impact of comparable side chain variations in the loop region. In ECL2, there are two additional polar residues that could participate in such interactions: Q220 and S222. We assessed the role of Q220 in TM3/4 folding by constructing two point mutants that could have variable effects on side chain electrostatic interactions: Q220G and Q220N. However, neither removal of the polar side chain in the Q220G mutant nor truncation of side chain length by a methylene group in the Q220N mutant effected a significant change in hairpin mobility (Figure 3, Table 1), suggesting that the WT Q220 was not likely to be participating in ECL2 side chain−side chain interactions.

On the other hand, removal of the side chain hydroxyl group at S222 by substitution with Gly, in the native

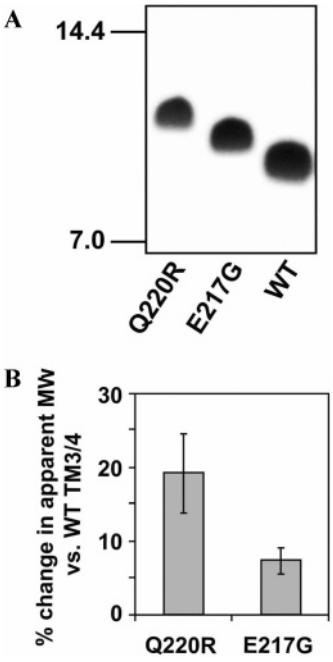

FIGURE 2: SDS−PAGE migration analysis of TM3/4 WT hairpins with and without CF-phenotypic mutations. (A) SDS−PAGE of TM3/4 WT and TM3/4 WT with E217G and with Q220R. (B) Analysis of the migration behavior of mutants vs WT by the percent change in apparent molecular weight on SDS−PAGE compared to that of WT (see Experimental Procedures for details).

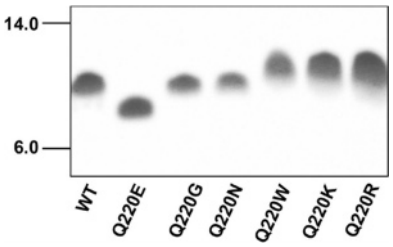

FIGURE 3: SDS−PAGE migration analysis of Q220 mutants in the TM3/4 WT background. 1 μg of protein was applied to each lane. Coomassie blue staining was used to visualize protein bands. The Q220E replacement migrates faster than TM3/4 WT, the Q220G and Q220N mutants migrate at equivalent rates to TM3/4 WT, while the Q220W, Q220K, and Q220R substitutions migrate more slowly. Values of percent decrease in molecular weight (Table 1) were calculated as described in Experimental Procedures.

background of E217, produced a helical hairpin that migrated more slowly than TM3/4 WT on SDS−PAGE and was thus considered to have disrupted structure (Table 1). We therefore hypothesized that the S222/E217 pair might form an intraloop interaction that stabilizes the native hairpin conformation and systematically replaced each side chain with Gly in the double mutant cycle consisting of S222G, E217G, S222G/E217G, and E217S/S222E. The unequal migration rates of the S222G and E217G hairpins in this cycle (6.8 ± 0.7 vs 12.0 ± 2.1, $p = 0.015$), however, were inconsistent with an interaction between the two residues, and the double mutant E217S/S222E, where the positions of the hydrogen bond donor and acceptor are interchanged, exhibited the largest perturbation in hairpin compactness (percent increase of apparent molecular weight compared to wild type = 26%) than any others encountered in this work. We therefore concluded that the disruptive effects of substitutions at S222 and/or E217, among them the

Table 1: Migration Behavior on SDS−PAGE Gels of Single and Double Mutants in the Loop Region of CFTR TM3/4 Constructs

mutant	% change in apparent MW on SDS−PAGE: vs TM3/4 WT in WT loop mutants[a]	% change in apparent MW on SDS−PAGE: vs TM3/4 V232D in V232D loop mutants[a]	P^b
E217G	6.8 ± 0.7		
E217S	11.1 ± 3.4	5.4 ± 1.4	0.056
Q220R	15.2 ± 1.1		
Q220G	0.3 ± 0.4		
Q220N	2.1 ± 1.3	0.5 ± 0.3	0.108
Q220K	14.1 ± 1.0		
Q220W	13.1 ± 1.3	11.5 ± 0.9	0.157
Q220E	**−11.1 ± 1.1**	**−4.0 ± 0.3**	<0.001
S222G	12.0 ± 2.1	1.1 ± 0.6	0.001
S222E	**−0.3 ± 2.4**	1.3 ± 0.5	0.512
E217G/S222G	12.4 ± 1.9		
E217S/S222E	26.1 ± 4.5		
average[c]	10.4 ± 7.3	4.0 ± 4.2	0.067

[a] Values are the percentage difference vs TM3/4 WT or TM3/4 V232D migration of SDS−PAGE gels. Negative values (in bold type) are for mutants that migrated faster than WT. Details of the calculation are described in Experimental Procedures. [b] Changes in the migration rates of the given ECL2 mutant in the TM3/4 WT or TM3/4 V231D background were compared using unpaired *t* tests. *P* values of 0.10 or less are deemed marginally statistically significant and values of 0.01 or less as highly statistically significant, with $p \leq 0.05$ the conventional standard of statistical significance. [c] The absolute values of the changes in the migration rates of all characterized mutants were averaged in the TM3/4 WT and TM3/4 V231D backgrounds. The mean and standard deviation are shown for each group. Means were compared using unpaired *t* tests, with $n = 12$ for WT and $n = 6$ for V231D.

CF-phenotypic replacement, could not be attributed solely a structural feature such as non-native H-bond formation.

Q220 Substitutions Can Decrease or Increase Hairpin Compactness. While Q220G- and Q220N-substituted hairpins migrate at the same rate as WT TM3/4, we undertook to examine this position systematically to determine the molecular determinants of migration rate variation. Thus, Q220 was replaced with Lys, Trp, and Glu in the TM3/4 WT background (Figure 3, Table 1). The Q220K and Q220W hairpins migrated identically to Q220R ($p = 0.259$ and $p = 0.101$, respectively) and to one another ($p = 0.341$), making it unlikely that the positive charge on the Arg side chain per se reduced hairpin compactness. The Q220E replacement, on the other hand, appeared to enhance the compactness of the TM3/4 WT hairpin.

α-*Helicity of ECL2-Substituted Hairpins Correlates with Gel Mobility.* To place the migration rates among our library of ECL2 mutants on a conformational basis, the secondary structure of each TM3/4 WT hairpin was examined by recording their CD spectra in SDS micelles, ostensibly conditions comparable to those imposed on the hairpins in SDS−PAGE gels. Earlier we had observed that TM3/4 constructs with lesions *within* their TM segments (e.g., WT vs I231D and V232D) display superimposible curves (*38*). By contrast, in the present work, we found categories of loop-mutant hairpins that could be distinguished spectroscopically by changes in their relative helicity as measured at 208 nm (Figure 4). Thus, the mutants that migrated more slowly than TM3/4 WT on SDS−PAGE gels, among them Q220R and E217S, generally displayed increased helicity compared to TM3/4 WT (Table 1, Figure 4A). On the other hand, mutants

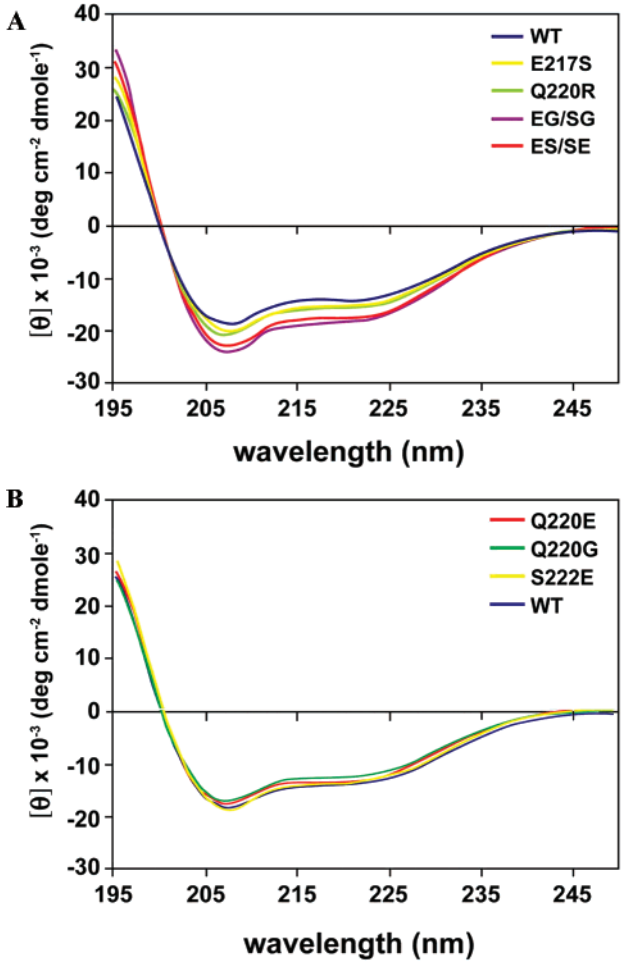

FIGURE 4: Circular dichroism spectra of TM3/4 WT helical hairpins in SDS micelles. (A) Spectra of selected mutants with slower than WT migration on SDS−PAGE. (B) Spectra of selected mutants with migration rates equal to or faster than WT. Spectra were recorded in 25 mM SDS in 10 mM Tris buffer at pH 7.5. Peptide concentration: 20 μM.

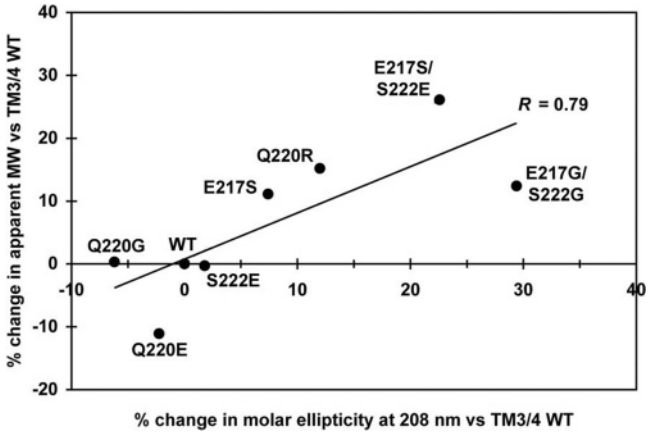

FIGURE 5: Least-squares plot of α-helicity vs TM3/4 WT hairpin gel mobility. Molar ellipticity values taken at 208 nm (see Figure 4) were plotted vs changes in apparent molecular weight relative to TM3/4 WT on SDS−PAGE gels (see Table 1).

that migrated similar to or faster than TM3/4 WT exhibited similar-to-WT helicity (Table 1, Figure 4B). When the changes in TM3/4 WT hairpin migration were compared to changes in overall hairpin helicity, a strong correlation ($R = 0.79$) was observed (Figure 5), leading us to propose that increases in non-native α-helix structure within ECL2 might

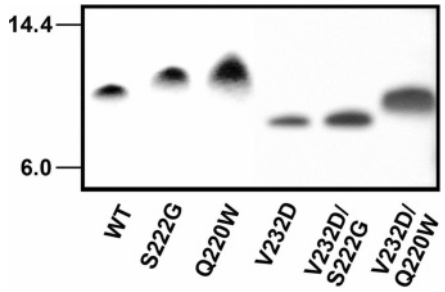

FIGURE 6: SDS−PAGE migration of S222G and Q220W replacements in the TM3/4 WT and TM3/4 V232D backgrounds. Hairpins containing ECL2 mutants S222G and Q220W in the TM3/4 WT background and in the TM3/4 V232D background are shown. 1 μg of protein was applied to each lane, and Coomassie blue staining was used to visualize protein bands. Values of percent decrease in molecular weight (Table 1) were calculated as described in Experimental Procedures.

mitigate against the compactness of helix−helix contacts within the TM3/4 WT hairpin structure.

ECL2 Mutants Are Less Disruptive in the Context of the Membrane-Based CF-Phenotypic TM Mutant V232D. If the helix−helix contacts in the TM3/4 WT hairpin are destabilized by an increase in α-helical structure in ECL2, then enhancement of stability of the membrane-embedded helix−helix interface might be expected to modulate the effect of loop mutations on overall hairpin conformation. The CF-phenotypic V232D replacement in TM helix 4 has been suggested in the TM3/4 hairpin context to form a stabilizing interhelical hydrogen bond (*33*, *38*); the TM3/4 V232D construct has a more compact fold than the TM3/4 WT hairpin and consequently migrates faster on SDS−PAGE (*33*). Several ECL2 replacements characterized as described above in the TM3/4 WT background were recapitulated in the TM3/4 V232D hairpin (Figure 6, Table 1). We found that the Q220E, S222G, and E217S replacements exhibited a relatively less pronounced effect on migration in the TM3/4 V232D hairpin than the TM3/4 WT background with high ($p < 0.01$ for Q220E and S222G) or detectable but marginal ($p = 0.056$ for E217S) statistical significance. The Q220N and Q220W replacements also affected folding less in the TM3/4 V232D background than in the TM3/4 WT hairpin (Table 1). The mean change in migration of ECL2 mutants in the TM3/4 V232D hairpin was >2-fold smaller than the WT. The structural perturbations of ECL2 introduced by the loop mutations thus appeared to affect hairpin conformation to a lesser extent in the context of more stable TM−TM helix−helix interactions.

DISCUSSION

Helical Hairpin Constructs as Models for Membrane Protein Folding. While it may be preferable to perform structural investigations on intact membrane proteins, their often substantial size (ca. 168 kDa for CFTR), high hydrophobicity, and concomitant challenges in overexpression and purification make obtaining sufficient amounts of the full-length molecule for biophysical studies a significant challenge. This reality has encouraged us and others to develop the use of defined TM domain helix−loop−helix or "hairpin" constructs that can be prepared in milligram amounts, manipulated readily by established biophysical techniques, and can accordingly be used to characterize the molecular events that link disease to phenotypic mutations. Hairpins represent the minimal model of *tertiary* contacts between two helices in a membrane and, as such, can recapitulate native helix−helix and loop conformations. Even when excised from the protein, individual TM segments have been shown to behave as independent folding domains and to retain their native contacts (*42*−*44*). Loop regions in hairpin constructs can also adopt relatively native conformations; for example, Ma and co-workers noted that the NMR structure of a TM2−loop−TM3 construct of the human glycine receptor α-1 subunit was in "striking agreement" with a full-length X-ray structure (*45*), and loop conformations consistent with full-length TM proteins have been observed in several other hairpin constructs (*46*, *47*). In addition, "truncated TM domains" such as hairpins can provide complementary atomic resolution structural information that cannot be obtained by any other existing methods (*45*) and are of modest molecular weights such that structural defects induced by mutations become readily detectable by gel and spectroscopic analysis; the structural defect of the same lesions in the full-length protein could lie below the detection levels of these techniques.

Evaluating CFTR Folding Using Helical Hairpins and SDS−PAGE Migration Assays. Determination of precise loop length remains a constant challenge, since it is difficult to specify at which residue a protein chain enters or exits a bilayer headgroup region (*34*). Prediction programs such as TM Finder are thus at best guidelines for definition of helix entry and exit points. We opted in the present work to consider the most inclusive ECL2 loop; this choice simultaneously reduced the expected length of the TM4 helix in the designed constructs. In any case, hairpins with relatively short loops (such as the ECL between CFTR TM3 and TM4) are expected to be tightly folded (*48*, *49*) and the most likely to retain native contacts.

The SDS−PAGE migration assays for TM3/4 developed in earlier work (*33*, *36*−*38*, *48*), where more compact hairpins ("closed" conformation) migrate *faster* than the corresponding elongated ("open" or more rod-like) forms of the protein, derive from the extent of folded tertiary structure that persists in SDS micelles. Like TM3/4, other proteins, such as cGMP-dependent protein kinase (*49*) and zinc regulatory factor (*50*), show conformation-dependent changes in mobility in PAGE systems where folding is maintained, with elongated forms migrating more slowly than compact forms. For the present study, TM3/4 constructs were examined in SDS micelles because the acknowledged disruptive nature of this detergent permits the detection of differences in interhelical packing that may be masked in other membrane-mimetic environments. Studies in SDS have the additional advantage of readily correlating gel migration with CD spectroscopy, as SDS micelles exhibit lower light scattering effects than other detergents (*51*). In this context, it is interesting to note that several members of the present library of TM3/4 ECL2 mutants migrate more slowly than the WT construct, indicating that sufficient noncovalent helix−helix contacts persist for WT TM3/4 in SDS to maintain a folded hairpin structure.

Influence of Charge on Hairpin Migration Rates. Distinguishing between migration pattern changes due to elongated vs compact conformations and those due to charge alteration is central to the SDS−PAGE assay. Several sets of experi-

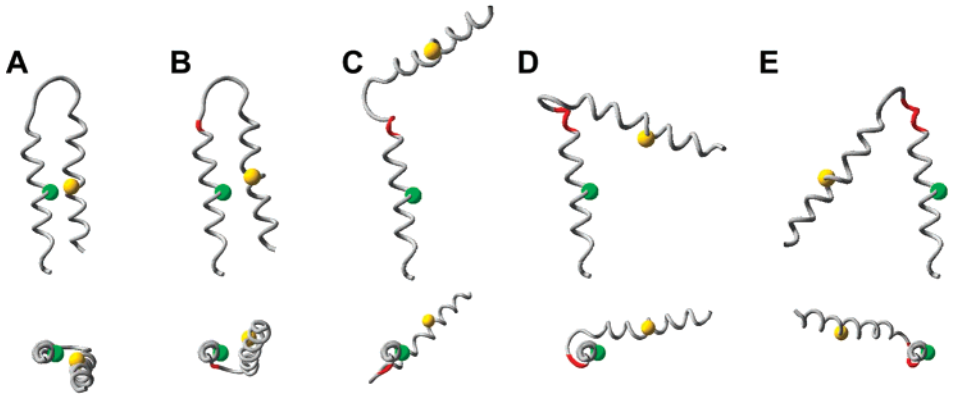

FIGURE 7: Disruption of helix−helix interactions by increased α-helical structure in the extracellular loop. The polypeptide backbone of a model helix hairpin is shown in (A) as a ribbon diagram, viewed perpendicular (top panel) and parallel (bottom panel) to the axis of the first helix. A pair of α-carbon atoms that could participate in interhelix contacts is shown in ball-and-stick representation. In (A), the backbone dihedral angles at the first 16 positions (helix 1, α-carbon in green) and final 19 positions (helix 2, α-carbon in yellow) were assigned α-helical values, and the intervening nine loop positions (gray) were assigned nonregular structure. In panels B−E, successive loop positions at the end of the first helix were assigned to the α-helical conformation (indicated by red shading), such that (B) has a single helical residue, (C) has two consecutive helical residues, and (E) has up to four. The increasing α-helix structure in the loop region forces apart the TM helices, swinging helix 2 out of the plane of the page to the left, eventually placing helix 2 on the side opposite from its original position. Interactions between specific residue side chains (such as H-bonds) and/or structural propensities of the actual residues in the TM3/4 loop were not considered. Figure produced using the SwissPDB Viewer (*52*).

ments suggest that TM3/4 migration patterns are not simple functions of charge: (i) The double mutant Q207L/V232D migrates identically to WT, while V232D migrates significantly faster than WT (*33*). (ii) Single Asp substitutions at 20 different positions between TM3/4 residues 221−241 exhibit a range of gel shift variations (3−12% faster than WT) (*38*); if introduction of a single negative charge was the dominating effect, all 20 mutants should display similar migration rates. (iii) TM3/4 mutants G241D (*38*) and G241R (data not shown) migrate within 2% of WT.

While there may be a potential charge factor in the migration patterns for certain Q220 mutations (Q220E, Q220K, and Q220R; Figure 3), the migration rates of other ECL2 mutants cannot be rationalized as simple functions of adding or subtracting single charges. For example, S222E and WT migrate at approximately the same rate, but Q220E moves at −11% vs WT; both S222G and E217G/S222G are at +12%; Q220K, Q220R, and Q220W are each at +13−15%. Moreover, in construct E217S/S222E, the net charge is not changed vs WT, yet the mutant runs at +26%. It may be further remarked that polar side chains that occur in ECL2, as well as those present in the S tag and His tag inherent in the expression vector, are all exposed to aqueous solvent and, as such, should be well solvated at pH 7.5 and unlikely to influence gel mobility on the basis of charge per se; a control construct in the S tag prepared to test this suggestion, Q15R, migrates similarly to WT TM3/4 (data not shown). As well, migration rates and spectroscopic determinations are performed with these tags uniformly as "background" in all hairpins, so the results obtained are normalized for their presence. These overall considerations suggest that the gel migration patterns among ECL2 mutants are not likely to be a function of charge but are instead influenced by conformational differences.

Mechanism of TM3/4 Structure Perturbation by CF-Phenotypic Mutants. Given the direct correlation between slower migration on SDS−PAGE and increasing hairpin α-helix content (Figure 4), we suspect that the ECL2 mutants destabilize the compact TM3/4 conformation by forcing the loop into a more helical conformation. Consequently, the decreased mobility of various TM3/4 WT constructs by introduction of non-native residues at E217 and/or Q220 is consistent with an elongation or "opening" of the helical hairpin and concomitant destabilization of membrane-based helix−helix interactions (*33*, *36*−*38*, *48*). These loop mutations may be extending the TM3 and/or TM4 helix structure into the ECL2 region, or additional residues in the ECL2 itself may adopt α-helical conformation. The structural consequences of either option are potentially drastic. For example, if an α-helical backbone conformation is assigned to a single residue at the first position of an unstructured loop in a model hairpin, the helices are forced apart in the absence of interhelical interactions (Figure 7, compare panel A vs panel B). This effect becomes more pronounced when successive residues are assigned α-helix structure (Figure 7C−E) and completely reorients the two helices with respect to one another. A similar disruption of the hairpin structure is observed when α-helical backbone assignments are made at the last residue in the loop region, or toward the middle of the loop sequence (not shown).

The TM3/4 V232D construct exhibits marginal but discernibly smaller migration changes than TM3/4 WT when ECL2 substitutions are introduced (Table 1, Figure 6). The stronger helix−helix interactions in TM3/4 V232D may therefore help to maintain a compact hairpin structure when ECL2 loop mutants are introduced that otherwise destabilize the fold. The stability of membrane protein folds in vivo may similarly reflect a balance between loop conformation and helix−helix interactions. While conformational changes induced by ECL2 mutants in the TM3/4 hairpin should be minimized by additional intrachain contacts imposed by the full-length CFTR molecule, our results suggest that the molecular mechanism of disease introduced by the CF-phenotypic ECL2 mutants E217G and Q220R may involve introduction of non-native α-helical loop structure that destabilizes the CFTR fold and leads to aberrant function in the resting state and/or during substrate transport.

CONCLUSION

While the present results implicate increased α-helical content in TM3/4 as the consequence of CF-phenotypic mutations, the precise link between side chain identity and this structural defect remains to be determined. These mutations thus have the potential to destabilize the native TM helix 3−TM helix 4 contacts that are required for normal channel function. Loop mutations are also shown using this assay to exert smaller effects in a mutant construct with strengthened TM helix 3−TM helix 4 interactions. Our results support a role for short loop regions in dictating the stability of membrane protein folds and highlight the interplay between helix−helix interactions and loop conformation in modulating membrane protein stability.

REFERENCES

1. Wallin, E., and von Heijne, G. (1998) Genome-wide analysis of integral membrane proteins from eubacterial, archaean, and eukaryotic organisms, *Protein Sci. 7*, 1029−1038.
2. Stevens, T. J., and Arkin, I. T. (2000) Do more complex organisms have a greater proportion of membrane proteins in their genomes?, *Proteins 39*, 417−420.
3. Gurrath, M. (2001) Peptide-binding G protein-coupled receptors: new opportunities for drug design, *Curr. Med. Chem. 8*, 1605−1648.
4. Partridge, A. W., Therien, A. G., and Deber, C. M. (2004) Missense mutations in transmembrane domains of proteins: phenotypic propensity of polar residues for human disease, *Proteins 54*, 648−656.
5. Oberai, A., Ihm, Y., Kim, S., and Bowie, J. U. (2006) A limited universe of membrane protein families and folds, *Protein Sci. 15*, 1723−1734.
6. Bowie, J. U. (2005) Solving the membrane protein folding problem, *Nature 438*, 581−589.
7. White, S. H. (2004) The progress of membrane protein structure determination, *Protein Sci. 13*, 1948−1949.
8. Popot, J. L., and Engelman, D. M. (1990) Membrane protein folding and oligomerization: the two-stage model, *Biochemistry 29*, 4031−4037.
9. Popot, J. L., and Engelman, D. M. (2000) Helical membrane protein folding, stability, and evolution, *Annu. Rev. Biochem. 69*, 881−922.
10. Liao, M. J., London, E., and Khorana, H. G. (1983) Regeneration of the native bacteriorhodopsin structure from two chymotryptic fragments, *J. Biol. Chem. 258*, 9949−9955.
11. Popot, J. L., Gerchman, S. E., and Engelman, D. M. (1987) Refolding of bacteriorhodopsin in lipid bilayers. A thermodynamically controlled two-stage process, *J. Mol. Biol. 198*, 655−676.
12. Kahn, T. W., and Engelman, D. M. (1992) Bacteriorhodopsin can be refolded from two independently stable transmembrane helices and the complementary five-helix fragment, *Biochemistry 31*, 6144−6151.
13. Marti, T. (1998) Refolding of bacteriorhodopsin from expressed polypeptide fragments, *J. Biol. Chem. 273*, 9312−9322.
14. Yu, H., Kono, M., McKee, T. D., and Oprian, D. D. (1995) A general method for mapping tertiary contacts between amino acid residues in membrane-embedded proteins, *Biochemistry 34*, 14963−14969.
15. Schoneberg, T., Liu, J., and Wess, J. (1995) Plasma membrane localization and functional rescue of truncated forms of a G protein-coupled receptor, *J. Biol. Chem. 270*, 18000−18006.
16. Berkower, C., and Michaelis, S. (1991) Mutational analysis of the yeast a-factor transporter STE6, a member of the ATP binding cassette (ABC) protein superfamily, *EMBO J. 10*, 3777−3785.
17. Zen, K. H., McKenna, E., Bibi, E., Hardy, D., and Kaback, H. R. (1994) Expression of lactose permease in contiguous fragments as a probe for membrane-spanning domains, *Biochemistry 33*, 8198−8206.
18. Gilles-Gonzalez, M. A., Engelman, D. M., and Khorana, H. G. (1991) Structure-function studies of bacteriorhodopsin XV. Effects of deletions in loops B-C and E-F on bacteriorhodopsin chromophore and structure, *J. Biol. Chem. 266*, 8545−8550.
19. Kahn, T. W., Sturtevant, J. M., and Engelman, D. M. (1992) Thermodynamic measurements of the contributions of helix-connecting loops and of retinal to the stability of bacteriorhodopsin, *Biochemistry 31*, 8829−8839.
20. Teufel, M., Pompejus, M., Humbel, B., Friedrich, K., and Fritz, H. J. (1993) Properties of bacteriorhodopsin derivatives constructed by insertion of an exogenous epitope into extra-membrane loops, *EMBO J. 12*, 3399−3408.
21. Allen, S. J., Kim, J. M., Khorana, H. G., Lu, H., and Booth, P. J. (2001) Structure and function in bacteriorhodopsin: the effect of the interhelical loops on the protein folding kinetics, *J. Mol. Biol. 308*, 423−435.
22. Kim, J. M., Booth, P. J., Allen, S. J., and Khorana, H. G. (2001) Structure and function in bacteriorhodopsin: the role of the interhelical loops in the folding and stability of bacteriorhodopsin, *J. Mol. Biol. 308*, 409−422.
23. Yeagle, P. L., Alderfer, J. L., Salloum, A. C., Ali, L., and Albert, A. D. (1997) The first and second cytoplasmic loops of the G-protein receptor, rhodopsin, independently form beta-turns, *Biochemistry 36*, 3864−3869.
24. Katragadda, M., Alderfer, J. L., and Yeagle, P. L. (2000) Solution structure of the loops of bacteriorhodopsin closely resembles the crystal structure, *Biochim. Biophys. Acta 1466*, 1−6.
25. Bennett, M., Yeagle, J. A., Maciejewski, M., Ocampo, J., and Yeagle, P. L. (2004) Stability of loops in the structure of lactose permease, *Biochemistry 43*, 12829−12837.
26. Piserchio, A., Bisello, A., Rosenblatt, M., Chorev, M., and Mierke, D. F. (2000) Characterization of parathyroid hormone/receptor interactions: structure of the first extracellular loop, *Biochemistry 39*, 8153−8160.
27. Giragossian, C., Schaschke, N., Moroder, L., and Mierke, D. F. (2004) Conformational and molecular modeling studies of beta-cyclodextrin-heptagastrin and the third extracellular loop of the cholecystokinin 2 receptor, *Biochemistry 43*, 2724−2731.
28. Riordan, J. R. (2005) Assembly of functional CFTR chloride channels, *Annu. Rev. Physiol. 67*, 701−718.
29. Seibert, F. S., Jia, Y., Mathews, C. J., Hanrahan, J. W., Riordan, J. R., Loo, T. W., and Clarke, D. M. (1997) Disease-associated mutations in cytoplasmic loops 1 and 2 of cystic fibrosis transmembrane conductance regulator impede processing or opening of the channel, *Biochemistry 36*, 11966−11974.
30. Seibert, F. S., Linsdell, P., Loo, T. W., Hanrahan, J. W., Riordan, J. R., and Clarke, D. M. (1996) Cytoplasmic loop three of cystic fibrosis transmembrane conductance regulator contributes to regulation of chloride channel activity, *J. Biol. Chem. 271*, 27493−27499.
31. Seibert, F. S., Linsdell, P., Loo, T. W., Hanrahan, J. W., Clarke, D. M., and Riordan, J. R. (1996) Disease-associated mutations in the fourth cytoplasmic loop of cystic fibrosis transmembrane conductance regulator compromise biosynthetic processing and chloride channel activity, *J. Biol. Chem. 271*, 15139−15145.
32. Hammerle, M. M., Aleksandrov, A. A., and Riordan, J. R. (2001) Disease-associated mutations in the extracytoplasmic loops of cystic fibrosis transmembrane conductance regulator do not impede biosynthetic processing but impair chloride channel stability, *J. Biol. Chem. 276*, 14848−14854.
33. Therien, A. G., Grant, F. E., and Deber, C. M. (2001) Interhelical hydrogen bonds in the CFTR membrane domain, *Nat. Struct. Biol. 8*, 597−601.
34. Deber, C. M., Wang, C., Liu, L. P., Prior, A. S., Agrawal, S., Muskat, B. L., and Cuticchia, A. J. (2001) TM Finder: a prediction program for transmembrane protein segments using a combination of hydrophobicity and nonpolar phase helicity scales, *Protein Sci. 10*, 212−219.
35. Peng, S., Liu, L. P., Emili, A. Q., and Deber, C. M. (1998) Cystic fibrosis transmembrane conductance regulator: expression and helicity of a double membrane-spanning segment, *FEBS Lett. 431*, 29−33.
36. Therien, A. G., and Deber, C. M. (2002) Interhelical packing in detergent micelles. Folding of a cystic fibrosis transmembrane conductance regulator construct, *J. Biol. Chem. 277*, 6067−6072.
37. Therien, A. G., Glibowicka, M., and Deber, C. M. (2002) Expression and purification of two hydrophobic double-spanning membrane proteins derived from the cystic fibrosis transmembrane conductance regulator, *Protein Expression Purif. 25*, 81−86.
38. Choi, M. Y., Cardarelli, L., Therien, A. G., and Deber, C. M. (2004) Non-native interhelical hydrogen bonds in the cystic fibrosis transmembrane conductance regulator domain modulated by polar mutations, *Biochemistry 43*, 8077−8083.

39. Riordan, J. R., Rommens, J. M., Kerem, B., Alon, N., Rozmahel, R., Grzelczak, Z., Zielenski, J., Lok, S., Plavsic, N., Chou, J. L., et al. (1989) Identification of the cystic fibrosis gene: cloning and characterization of complementary DNA, *Science 245*, 1066−1073.
40. Wigley, W. C., Vijayakumar, S., Jones, J. D., Slaughter, C., and Thomas, P. J. (1998) Transmembrane domain of cystic fibrosis transmembrane conductance regulator: design, characterization, and secondary structure of synthetic peptides m1-m6, *Biochemistry 37*, 844−853.
41. Bond, P. J., Holyoake, J., Ivetac, A., Khalid, S., and Sansom, M. S. (2007) Coarse-grained molecular dynamics simulations of membrane proteins and peptides, *J. Struct. Biol. 157*, 593−605.
42. Melnyk, R. A., Partridge, A. W., and Deber, C. M. (2001) Retention of native-like oligomerization states in transmembrane segment peptides: application to the *Escherichia coli* aspartate receptor, *Biochemistry 40*, 11106−11113.
43. Partridge, A. W., Melnyk, R. A., Yang, D., Bowie, J. U., and Deber, C. M. (2003) A transmembrane segment mimic derived from Escherichia coli diacylglycerol kinase inhibits protein activity, *J. Biol. Chem. 278*, 22056−22060.
44. Rath, A., Melnyk, R. A., and Deber, C. M. (2006) Evidence for assembly of small multidrug resistance proteins by a "two-faced" transmembrane helix, *J. Biol. Chem. 281*, 15546−15553.
45. Ma, D., Liu, Z., Li, L., Tang, P., and Xu, Y. (2005) Structure and dynamics of the second and third transmembrane domains of human glycine receptor, *Biochemistry 44*, 8790−8800.
46. Katragadda, M., Alderfer, J. L., and Yeagle, P. L. (2001) Assembly of a polytopic membrane protein structure from the solution structures of overlapping peptide fragments of bacteriorhodopsin, *Biophys. J. 81*, 1029−1036.
47. Ulfers, A. L., McMurry, J. L., Kendall, D. A., and Mierke, D. F. (2002) Structure of the third intracellular loop of the human cannabinoid 1 receptor, *Biochemistry 41*, 11344−11350.
48. Choi, M. Y., Partridge, A. W., Daniels, C., Du, K., Lukacs, G. L., and Deber, C. M. (2005) Destabilization of the transmembrane domain induces misfolding in a phenotypic mutant of cystic fibrosis transmembrane conductance regulator, *J. Biol. Chem. 280*, 4968−4974.
49. Chu, D. M., Francis, S. H., Thomas, J. W., Maksymovitch, E. A., Fosler, M., and Corbin, J. D. (1998) Activation by autophosphorylation or cGMP binding produces a similar apparent conformational change in cGMP-dependent protein kinase, *J. Biol. Chem. 273*, 14649−14656.
50. Otsuka, F., Okugaito, I., Ohsawa, M., Iwamatsu, A., Suzuki, K., and Koizumi, S. (2000) Novel responses of ZRF, a variant of human MTF-1, to in vivo treatment with heavy metals, *Biochim. Biophys. Acta 1492*, 330−340.
51. Lazarova, T., Brewin, K. A., Stoeber, K., and Robinson, C. R. (2004) Characterization of peptides corresponding to the seven transmembrane domains of human adenosine A2a receptor, *Biochemistry 43*, 12945−12954.
52. Guex, N., and Peitsch, M. C. (1997) SWISS-MODEL and the Swiss-PdbViewer: an environment for comparative protein modeling, *Electrophoresis 18*, 2714−2723.

BI602570U